Progress in Gyrokinetic Simulations of Toroidal ITG Turbulence.[1]

A.M. DIMITS, B.I. COHEN, W.M. NEVINS, D.E. SHUMAKER

[1)] Lawrence Livermore National Laboratory Livermore, CA 94551, USA

e-mail contact of main author: dimits1@llnl.gov

Abstract. The 3-D nonlinear toroidal gyrokinetic simulation code PG3EQ is used to study toroidal ion temperature gradient (ITG) driven turbulence – a key cause of the anomalous transport that limits tokamak plasma performance. Systematic studies of the dependence of ion thermal transport on various parameters and effects are presented, including dependence on $\vec{E} \times \vec{B}$ and toroidal velocity shear, sensitivity to the force balance in simulations with radial temperature gradient variation, and the dependences on magnetic shear and ion temperature gradient.

1. Introduction, Simulation Code and Parameters

Toroidal ion temperature gradient (ITG) driven turbulence is considered a key cause of the anomalous transport that limits tokamak plasma performance. However, existing ITG-based transport models are either derived from highly reduced dynamical models or depart from nonlinear gyrokinetic predictions [1]. This motivates more extensive and systematic nonlinear gyrokinetic simulation studies of transport due to such turbulence.

The LLNL 3-D nonlinear toroidal gyrokinetic simulation code PG3EQ [2] is a product of advances in simulation algorithms (δf solution of the toroidal nonlinear gyrokinetic Vlasov equation, the "quasiballooning" numerical representation, and flux-tube simulation domains). This, along with rapid growth in available computer power, has made PG3EQ a practical tool for studying ITG microturbulence for realistic plasma parameters.

The details of the code, the problem setup, typical numerical parameters, and the definition of the normalized ion thermal conductivity used are as described in Ref. [3]. Table I shows base values of the physical parameters used here. Their definitions are standard and are given, e.g., in Ref. [2]. Their values correspond to experimental conditions or test cases described respectively in Refs. [4] (Cyclone) and [5] (NTTP).

2. Effect of External Velocity Shear

The external $\vec{E} \times \vec{B}$ shear is treated, using the quasiballooning representation [2] with coordinates which shear with the external $\vec{E} \times \vec{B}$ shear field in addition to the magnetic shear [2]. This approach is optimally efficient, avoids any nonphysical boundary effects, and has no difficulty at zero magnetic shear S.

The results, shown in Fig. 1, show several notable departures from the $\vec{E} \times \vec{B}$-shear turbulence-quenching model [6] [$\chi_i \propto \max(0, [1 - C|\vec{V}'_{EB}|/\gamma_{max}])$, where $C \simeq 4/3$, $\vec{V}'_{EB}$ is the external $\vec{E} \times \vec{B}$ shearing rate, and γ_{max} the maximum linear growth rate for $\vec{V}'_{EB} = 0$].

[1]Work performed under the auspices of the U. S. Department of Energy by University of California Lawrence Livermore National Laboratory under contract W-7405-ENG-48.

case	$\eta_{\rm i}$	q	S	$R/L_{\rm Ti}$	ϵ_B	$T_{\rm i}/T_{\rm e}$
Cyclone	3.114	1.4	0.78	6.92	0.18	1.0
NTTP	4.0	2.4	1.6	10.0	0.2057	1.0
NTTP-$S=0$	4.0	2.4	0.0	10.0	0.2057	1.0
NTTP-$\epsilon_B=0$	4.0	2.4	1.6	10.0	0.0	1.0
NTTP-$q=1.6$	4.0	1.6	1.6	10.0	0.2057	1.0

TAB. I: *Simulation parameters used as base cases for scans.*

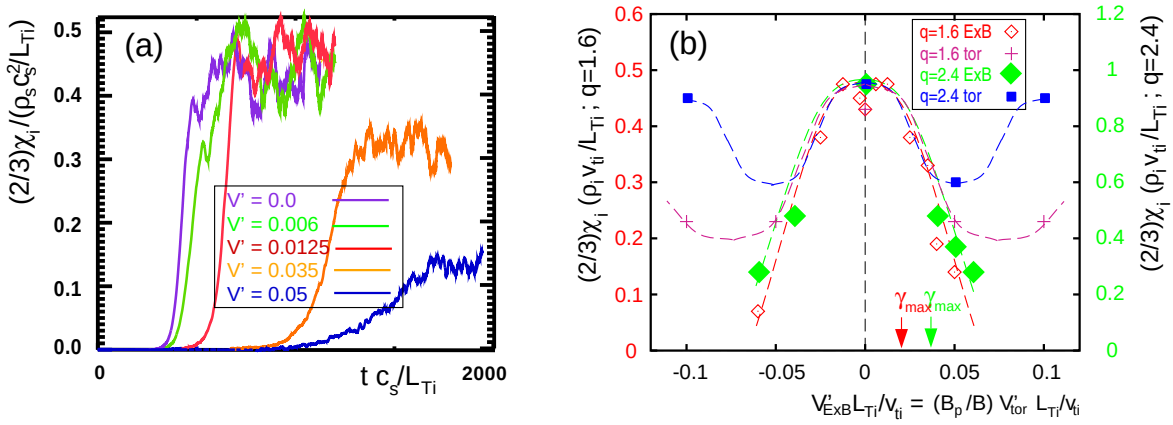

FIG. 1: (a) Time histories of $\chi_{\rm i}$ for different values of the $\vec{E}\times\vec{B}$ shear, for the $q=1.6$-NTTP case, and (b) dependence of $\chi_{\rm i}$ on external $\vec{E}\times\vec{B}$ and toroidal shearing rates for scans about the NTTP and NTTP-$q=1.6$ cases.

Firstly, for magnetic safety factor $q=1.6$ there is a plateau range of values of $\vec{V}'_{\rm EB}$ for which $\chi_{\rm i}$ is not reduced (but the maximum linear growth rate is), so that the onset of transport reduction is more sudden than given by the quenching model. Secondly, when the NTTP ($q=2.4$) and NTTP-$q=1.6$ points are scaled and overlayed, the two sets of points approximately track each other, and therefore extrapolate to zero $\chi_{\rm i}$ at similar values $\vec{V}'_{\rm EB0}\simeq 0.075\pm 0.005$ of $\vec{V}'_{\rm EB}$. This is significantly larger than and scales differently with q than does $\gamma_{\rm max}$.

Closer examination reveals that as $\vec{V}'_{\rm EB}$ is increased in the plateau region, it supplants some of the self-generated $\vec{E}\times\vec{B}$ shear ("zonal flows") so that the effective $\vec{E}\times\vec{B}$ shearing rate remains roughly constant. In contrast, in the simulations of Ref. [6] the zonal flows are overdamped [7], so lower values of $\vec{V}'_{\rm EB}$ more immediately reduce $\chi_{\rm i}$.

Figure 1(b) also shows $\chi_{\rm i}$ vs. applied toroidal ($\vec{E}\times\vec{B}$ + parallel) velocity shear $\vec{V}'_{\rm tor}$. For sufficiently small $\vec{V}'_{\rm tor}$ the points track those for pure $\vec{E}\times\vec{B}$ shear. However, for larger $\vec{V}'_{\rm tor}$, $\chi_{\rm i}$ increases and (e.g., for the NTTP-case scan) can attain values similar to those for $\vec{V}'_{\rm tor}=0$.

3. Equilibrium-Profile-Scale Effects

Global simulations of ITG turbulence [8] suggest that ion temperature gradient [$T'_{\rm i}(r)$] variation is the most important profile-scale effect. In previous simulations with radial

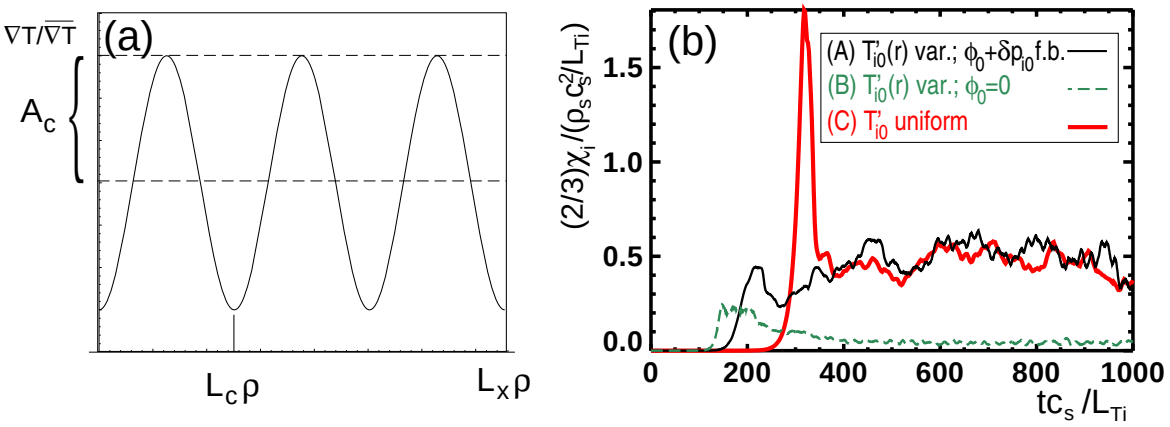

FIG. 2: (a) Diagram of temperature-gradient profile and parameters and (b), time histories of χ_i for simulations (A) with initial radial temperature-gradient variation and with initial radial force balance between the radial electric field and the ion pressure, (B) with radial temperature-gradient variation and ϕ initialized to zero (green), and (C) no initial radial temperature-gradient variation (blue).

variation in $T_i'(r)$ [8, 3], the elecrostatic potential ϕ was initially negligible. We use a new method for quietly initializing the simulations with profile variation and matching the neoclassical expectation [9] of the net (electric + pressure) radial force being small in much of the plasma.

Figure 2 compares such a simulation (A) with a simulation (B) with the same initial $T_i'(r)$ profile but with ϕ initialized to zero, and with a simulation (C) initialized with no radial $T_i'(r)$ variation, but the same radially averaged $T_i'(r)$. The Cyclone-case parameters were used. The radially varying $T_i'(r)$ profiles were chosen as $T_i'(r) = T_{i0}'[1+\delta\cos 2\pi(r-r_0)/\Delta_x]$, with $\Delta_x = 42\rho_i$, where ρ_i is the mean ion gyroradius, and $\delta = 0.75$. The radial system size is $125\rho_i$. In the simulation (B), it is seen that χ_i goes essentially to zero at late time. In contrast, χ_i in simulation (A) approaches a value similar to that in the simulation without any $T_i'(r)$ variation.

A more detailed examination shows that the nonlinear evolution of simulations (A) and (B), preserves $e\phi/T_e + p/p_0$, where $-e$ and T_e are the electron charge and temperature, and p and p_0 are the radially varying and mean equilibrium pressures. In both simulations (A) and (B) most of the radial variation of the temperature decays away due to nonlinear processes. In simulation (B), the approximate preservation of the radial force implies a self-generated radially varying radial electric field which inhibits the turbulent transport. In contrast, in simulation (A) the radial variations in the temperature and in the electrostatic potential decay away, so that there is little radial electric field and the late time state is very similar to that in simulation (C) which had no initial $T_i'(r)$ variation. Thus, previous conclusions, e.g., in Ref. [8], that $T_i'(r)$ variations quench toroidal ITG turbulence need to be qualified with a more careful examination of how the scheme that generates the $T_i'(r)$ variation affects the radial force balance.

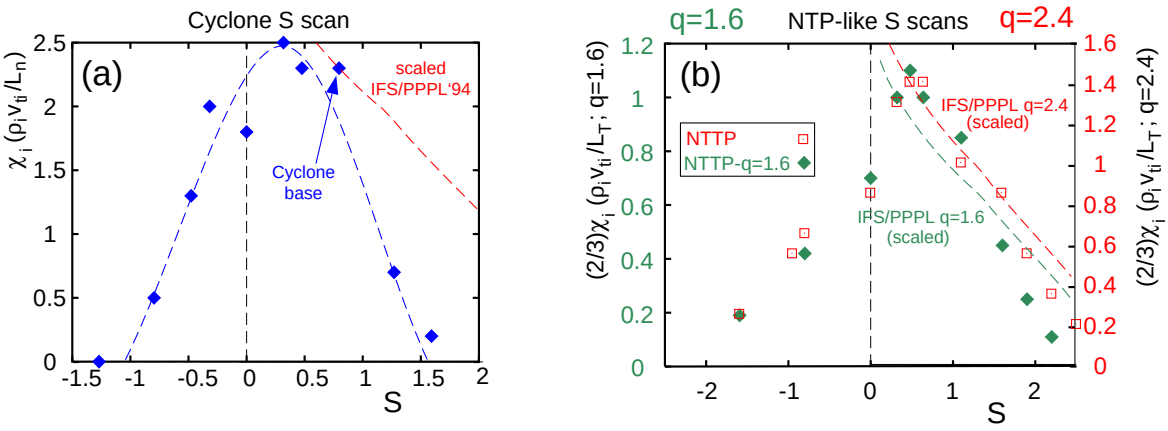

FIG. 3: χ_i vs. S for scans in S about (a) the Cyclone parameters and (b) NTTP and NTTP-$q = 1.6$ parameters. Also shown are the predictions of the IFS/PPPL'94 transport model.

4. Dependence of χ_i on S

Figure 3 shows the results from three scans in $S = (r/q)dq/dr$. A clear peak in χ_i vs. S is observed at around $S \simeq 0.5$, which is very sharp for the NTTP-based scans. Furthermore, the effect of changing q from 2.4 to 1.6 is well represented by a single multiplicative factor applied to χ_i.

Figure 3 also shows that the 1994 IFS/PPPL model [10] (the version that most closely represents the results of nonlinear gyrofluid simulations) matches the trend of NTTP-based scans reasonably well for $S \gtrsim 0.5$ but not for $S < 0.5$. The 1994 IFS/PPPL model does not predict the shear dependence in the Cyclone-based scan.

The value of $S \simeq 0.5$ at the peak is that at which orientation of the linear ITG modes is independent of poloidal angle in the region near the outer mid plane, and also shows the longest-spatial-scale correlations in the nonlinear phase.

5. Temperature Gradient Scans

Figure 4 shows results for four χ_i vs. R/L_{Ti} scans which sample quite different parts of the parameter space. A remarkably good fit to the dependence of the thermal *flux* on R/L_{Ti} for these scans can be obtained by an offset linear dependence on R/L_T, shown as the dashed lines.

These fits can be expressed as $\chi_i(L_n/\rho_s^2 c_s) = D_{\chi_i}[1 - (R/L_{Teff})/(R/L_{Ti})]$. For all of the above scans except the NTTP-$\epsilon_B = 0$ case, R/L_{Teff} is significantly greater than the normalized linear critical gradient R/L_{Tclin}. In the scans with $\epsilon_B \neq 0$, for $R/L_{Tclin} < R/L_{Ti} < R/L_{Teff}$ the simulations are linearly unstable, but the thermal transport at late time becomes essentially zero [3]. Interestingly in the Cyclone-$\epsilon_B = 0$ scan, the $R/L_{Teff} > R/L_{Tclin}$, phenomenon still persists. For R/L_{Ti} in this range, the thermal transport is nonzero but very small (i.e., $\chi_i(L_n/\rho_s^2 c_s) \ll D_{\chi_i}[1 - (R/L_{Tclin})/(R/L_{Ti})]$.

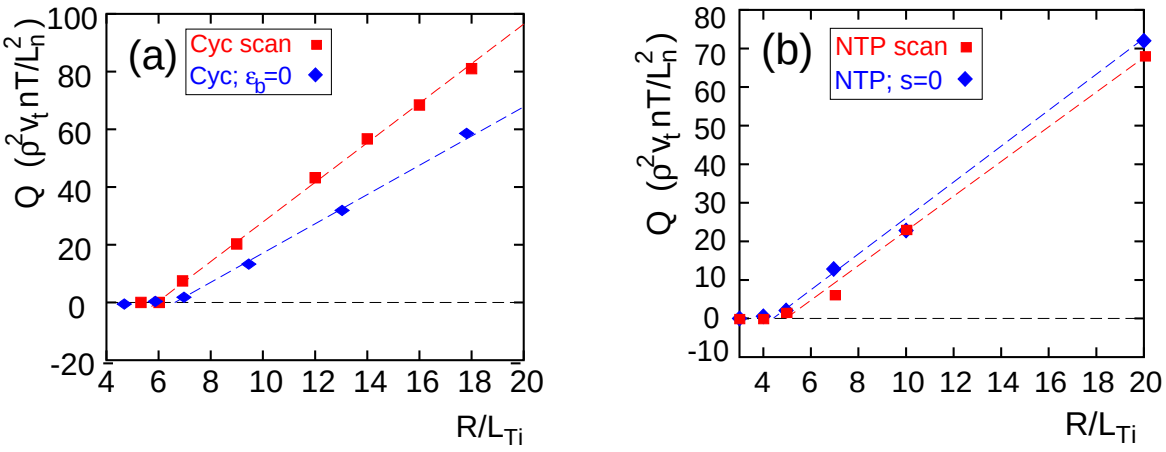

FIG. 4: Normalized ion thermal flux vs. $R/L_{\rm Ti}$ for $R/L_{\rm Ti}$ scans about (a) the Cyclone case (red squares) and Cyclone-$\epsilon_B = 0$ case (blue diamonds), (b) the NTTP case (red squares) and for the NTTP-$S = 0$ case (blue diamonds).

6. Acknowledgments

The simulations were done on the NERSC T3E. This work is part of the Plasma Microturbulence Project supported by the DOE OFES at the University of California Lawrence Livermore National Laboratory under contract W-7405-ENG-48.

References

[1] A.M. Dimits *et al.*, Phys. Plasmas **7**, 969 (2000).

[2] A. M. Dimits, T. J. Williams, J. A. Byers, and B. I. Cohen, Phys. Rev. Lett. **77**, 71 (1996), and references therein.

[3] A. M. Dimits *et al.*, in *Proc. 17th Int. Conf. on Fusion Energy*, Yokohama, 1998 (IAEA, Vienna, 1999); Nucl. Fusion **40**, 661 (2000).

[4] C.M. Greenfield, J.C. DeBoo, T.H. Osborne, F.W. Perkins , M.N. Rosenbluth, D. Boucher, Nuclear Fusion **37**, 1215 (1997).

[5] B. I. Cohen, D. C Barnes, J. M. Dawson,*et al.*, Comp. Phys. Commun. **87**, 1 (1995).

[6] R.E. Waltz, R.L. Dewar, and X. Garbet, Phys. Fluids **5**, 1784 (1998).

[7] M.N. Rosenbluth and F.L. Hinton, PRL **80**, 724 (1998).

[8] S. E. Parker, C. Kim, Y. Chen, Phys. Plasmas **6**, 1709 (1999).

[9] D. R. Ernst et al., Phys. Plasmas **5**, 665 (1998).

[10] W. Dorland et al., *Proc. 15th Int. Conf on Plasma Physics and Controlled Nuclear Fusion Research*, Seville, 1994, (IAEA, Vienna, 1995) Vol. 3, 463.